ELSEVIER

Earth and Planetary Science Letters 192 (2001) 175–189

EPSL

www.elsevier.com/locate/epsl

The transition from linear to diffuse plate boundary in the Azores–Gibraltar region: results from a thin-sheet model

Ivone Jiménez-Munt [a,*], Manel Fernàndez [a], Montse Torne [a], Peter Bird [b]

[a] *Institute of Earth Sciences 'J. Almera', C.S.I.C., Solé Sabarís s/n, 08028 Barcelona, Spain*
[b] *Department of Earth and Space Sciences, University of California, Los Angeles, CA 90095-1567, USA*

Received 27 February 2001; received in revised form 5 July 2001; accepted 10 July 2001

Abstract

We use the thin-sheet plane-stress approach to study the present-day dynamic behavior of the plate boundary between Eurasia and Africa along the Azores–Gibraltar region. This plate boundary, which extends from the Azores triple junction to the Gibraltar strait, shows a tectonic regime that changes from transtension in the west to transpression in the east, with a strike–slip motion in its central segment. Seismological data reveal that the western and central segments are currently marked by a linear series of earthquakes indicating that the plate boundary is located in a narrow zone. In contrast, the eastern segment is not so well defined and deformation spreads over a much broader area. To apply the thin-sheet approach, we combined heat flow, elevation and crustal thickness data to calculate the steady-state geotherm and the total strength of the lithosphere. Several models with different fault friction coefficients and geometries at the eastern segment of the plate boundary were tested. Results are compared with the maximum compressive stress directions from the World Stress Map, and the calculated seismic strain rates and slip vectors from earthquake data. The best fitting models are consistent with the rotation pole of Argus et al. [D.F. Argus et al., J. Geophys. Res. 94 (1989) 5585–5602], and show that the rheological behavior of the plate boundary must necessarily change from the western and central segments to the eastern segment. The diffuse character of the plate boundary east of the Gorringe Bank is dominated by the transition from oceanic to continental lithosphere, the weakness of the Alboran domain, and the convergence between the African and the Eurasian plates. The displacement of the Alboran domain relative to the African plate may play a major role in stress propagation through the Iberian Peninsula and its Atlantic margin.

Keywords: stress; strain; rotation; seismicity; neotectonics

1. Introduction

The Azores–Gibraltar region contains a major strike–slip structure that extends from the Azores triple junction to the Gibraltar strait in a W–E direction and separates the Eurasian and African plates (Fig. 1). Geophysical studies of the Azores triple junction suggest that the spreading rate of the Mid-Atlantic ridge south of the Azores Is-

* Corresponding author. Present address: Dipartimento di Scienze della Terra, Sezione Geofisica, Università degli Studi di Milano, via L. Cicognara 7, 20129 Milan, Italy. Tel.: +39-02-23698412; Fax: +39-02-7490588.
E-mail address: ivone.jimenez@unimi.it (I. Jiménez-Munt).

0012-821X/01/$ – see front matter
PII: S0012-821X(01)00442-3

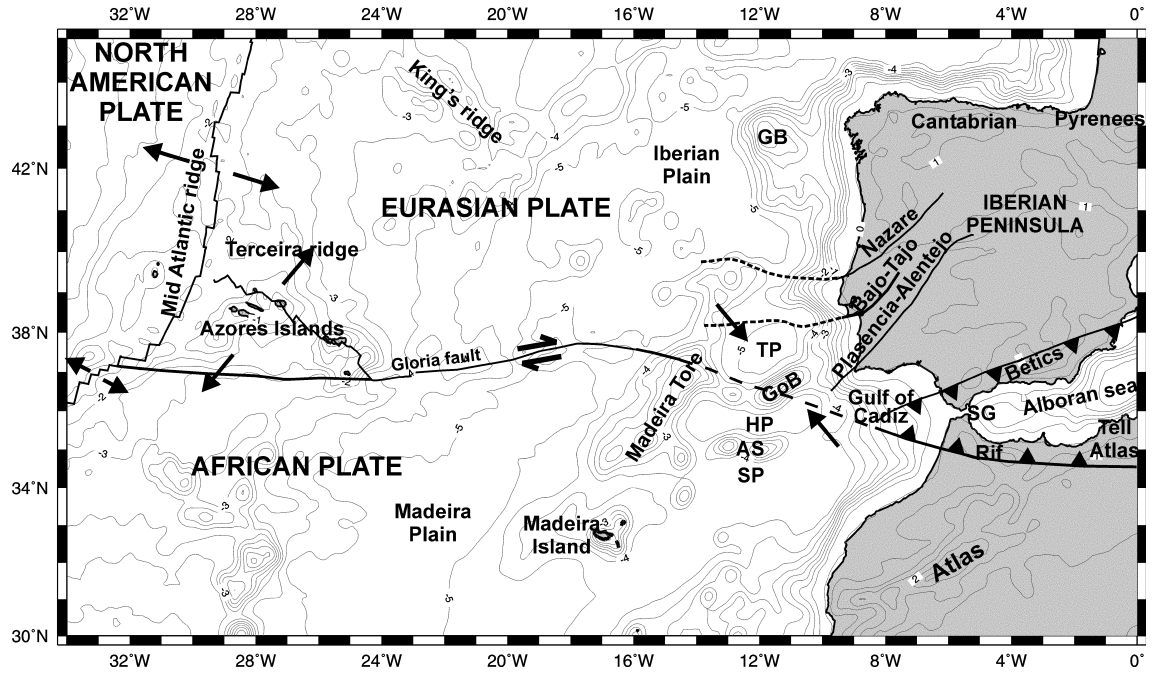

Fig. 1. Tectonic sketch map of the study region (modified from [2]). Abbreviations: GB: Galicia Bank; TP: Tagus Plain; GoB: Gorringe Bank; HP: Horseshoe Plain; AS: Ampere Seamount; SP: Seine Plain; SG: Strait of Gibraltar. Bathymetric contours every 500 m.

lands is lower than that observed in the northern segment, which results in a dextral transcurrent movement along the boundary. The Azores segment (Terceira ridge) has high seismicity of moderate magnitude and a low slip rate; the predominant mechanism is normal or transform faulting with horizontal tensions averaging N25°E [2]. The Gloria fault forms a seismic gap that extends from 24°W to 20°W. From 20°W to 13°W the boundary is E–W oriented with large earthquakes showing right lateral strike–slip motion. This region is currently marked by an alignment of earthquakes indicating that the plate boundary is located in a narrow zone. However, the easternmost segment (east of the Madeira Tore Rise) is more complex and the predominant mechanism is reverse faulting with a horizontal pressure axis around N30°W [2,3]. In this region, deformation spreads over a much wider area as evidenced by the presence of regional NE–SW and E–W oriented structures (e.g. Gorringe Bank and Ampere Seamount). Further to the east, in the continental domain, the plate boundary becomes more complex resulting in the Alboran Sea extensional basin, which is surrounded by the Betic and Rif cordilleras to the north and south, respectively. The Alboran basin shows a progressive crustal and lithospheric thinning towards the east [4] and opens to the oceanic domain of the South Balearic basin.

In summary, the Azores–Gibraltar plate boundary is very well defined in its western and central segments, whereas east of the Madeira Tore Rise there is a lack of consensus on its geometry and location as inferred from the variety of models proposed so far (e.g. [1–3,5–7]). Moreover, the kinematics along the plate boundary are consistent with a counterclockwise rotation of the African plate relative to the Eurasian plate [1,8].

The main goal of this paper is to define the geometry of the Azores–Gibraltar plate boundary with special emphasis in the transition from the linear strike–slip central segment to the NNW–SSE compressive diffuse eastern segment. To this end, we used the thin-sheet plane-stress approach which allowed us to calculate the present-day kin-

ematics and dynamics of the region and to compare the resulting stress orientations and strain rates with available data. In addition, as plate-like kinematics depend strongly on the relevant rotation pole, our modelling results also indicate the best pole location from among those proposed by several authors.

2. Structure and strength of the lithosphere

The plane-stress approach assumes that the lithosphere behaves as a thin layer with a vertically averaged viscous rheology. The average viscosity and the total lithospheric strength are calculated from the yield stress envelope once the crustal and the lithospheric mantle thicknesses are known. The dynamic finite-difference code UHURU used in this work calculates the instantaneous lithospheric deformation and stress distribution by coupling the equilibrium and constitutive equations for a highly viscous fluid and considering the gravitational potential energy related to crustal and lithospheric mantle thickness variations (see Appendix).

Table 1
Parameters used in the calculations

ρ_c	Crustal density	2780 kg m^{-3}
ρ_a	Asthenospheric density	3200 kg m^{-3}
ρ_w	Water density	1032 kg m^{-3}
α	Volumetric thermal expansion coefficient of lithospheric mantle	3.5×10^{-5} K^{-1}
K_c	Thermal conductivity of crust	3.0 W m^{-1} K^{-1}
K_m	Thermal conductivity of lithospheric mantle	3.2 W m^{-1} K^{-1}
T_{sup}	Surface temperature ($z=0$)	0°C
T_a	Temperature at the base of the lithosphere ($z=L$)	1300°C
H_{sup}	Surface heat production:	
	If $0\leq e$	2.5×10^{-6} W m^{-3}
	If -500 m$\leq e<0$	1.25×10^{-6} W m^{-3}
	If $e<-500$ m	0.625×10^{-6} W m^{-3}
b	Exponential coefficient of the crustal heat production	15 000 m
H_m	Lithospheric mantle heat production	0 W m^{-3}
nx, ny	Number of horizontal nodes	51, 51

To determine the crustal and lithospheric mantle structure we assumed local isostasy, steady-state thermal regime, and that the base of the lithosphere is defined by the 1300°C isotherm. Under these conditions there is a non-linear relationship between absolute elevation, surface heat flow, crustal and lithospheric mantle thickness, such that knowledge of two of these variables allows us to calculate the two unknowns (see Appendix). Thereby, depending on the data available we used elevation and surface heat flow or, alternatively, elevation and crustal thickness, as input data to determine the lithospheric structure in the whole region.

Elevation was taken from the ETOPO-5 global dataset. In the Iberian Peninsula and its western margin, we used seismic data to constrain the crustal thickness, whereas in those areas with poor seismic coverage (e.g. North Africa) and in the oceanic domain we used surface heat flow values. Surface heat flow was taken from the global dataset of Pollack et al. [9], from Fernandez et al. [10] for the Iberian Peninsula and its margins, and from the global heat flow–age relationship [11] for the oceanic domain. Radiogenic heat production is considered to decay exponentially with depth and surface values vary for continental lithosphere, oceanic lithosphere, and shelf areas with large sedimentary accumulations. Table 1 shows the parameters used to calculate the regional crustal and lithospheric thickness variations shown in Fig. 2. Calculations were performed after filtering all the observables with a box-car filter of 100 km wavelength to remove local features. Therefore, these maps do not reflect the fine structure of the crust and mantle lithosphere but their resolution suffices to introduce relevant lateral variations of the total lithospheric strength and body forces. Although departures from local isostasy, as reported in the Gorringe Bank region [12], may result in misestimation of the actual lithospheric structure, the induced departures in the calculated lithospheric strength and the gravitational potential energy are negligible.

Crustal thicknesses of about 5 km are found in the abyssal plains of the oceanic domain increasing near the Azores Islands. A significant crustal

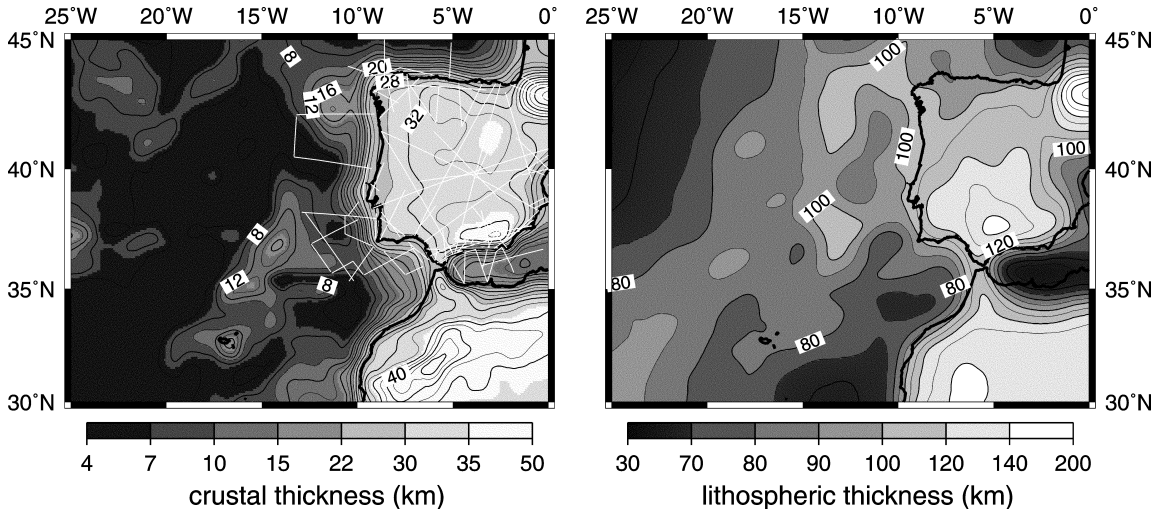

Fig. 2. (Left) Calculated crustal thickness (contours every 2.5 km) and used seismic profile data (white lines). (Right) Calculated lithospheric thickness (contours every 10 km).

thickening is observed along the Madeira Tore Rise and the Galicia Bank. This regional trend is in agreement with the observed Bouguer anomalies which show relative highs between the Mid-Atlantic ridge and the Madeira Tore Rise, in a NNE–SSW oriented band crossing the Gloria fault [12,13]. Towards the continental slope and shelf, the crust thickens to values of 25–30 km at the shoreline and maximum values occur underneath the Betics and Atlas, in agreement with available seismic data [14,15]. The lithospheric thickness reaches minimum values near the Mid-Atlantic ridge increasing progressively towards the Iberian margin. Short wavelength variations of small amplitude (± 10 km) are observed in the Madeira Tore Rise and Galicia Bank regions. Along the African margin, the lithosphere thins to values of less than 70 km thickening abruptly towards the African craton. This thinning, which is bounded by chron M25 to the west and the continental slope to the east, results from considering a surface heat flow of 60–65 mW m^{-2}, according to available data. The Alboran region shows large variations in lithospheric thickness, with maximum values below the Betics and northern Atlas and minimum values in the Alboran basin, in agreement with previous studies [4].

The resulting crustal and lithospheric structures allowed us to compute the lateral variations of the total strength of the lithosphere and its vertically averaged viscosity by considering a three layer rheology. The upper crust is considered to have a quartz dominated rheology and a thickness that is 2/3 of the total crustal thickness, whereas the lower crust is dominated by diabase composition. The lithospheric mantle is considered to be dominated by olivine rheology. Rheological parameters were taken from average values from different

Table 2
Rheological parameters [18]

	β (kPa m^{-1})	A (MPa^{-n} s^{-1})	n	Q (kJ mol^{-1})
Upper crust	40	2.5×10^{-8}	3	138
Lower crust	40	3.2×10^{-3}	3	251
Lithospheric mantle	40	1×10^{3}	3	523
Lithospheric mantle (Dorn law)	$\sigma_D = 8.5\times10^{9}$ Pa, $\dot{\varepsilon}_D = 5.7\times10^{11}$ s^{-1}, $Q_D = 100$ kJ mol^{-1}			
Strain rate	$\dot{\varepsilon} = 3.171\times10^{-16}$ s^{-1} (10 mm yr^{-1} over 1000 km)			

studies (e.g. [16,17]) and used as representative by Lynch and Morgan [18] (Table 2). Since total lithospheric strength is highly dependent on geotherm, the minimum values are along the Mid-Atlantic ridge, in the Alboran Sea basin, and along the African continental margin. In contrast, maximum values are along the Iberian Atlantic margin and southwestern Spain. It is relevant to note that no rheologically induced weak/stiff inclusions (e.g. [19,20]) are considered in the model. Therefore, the choice of the rheological parameters plays a secondary role since the model is sensitive to variations of lithospheric strength related to lateral changes in the crustal and lithospheric structure.

3. Kinematic constraints

Numerical results are constrained by comparing with different kinematic data: stress orientation, slip vector, and seismic strain rate (Fig. 3). To allow objective comparisons between alternative computed models we defined three misfit parameters:

(1) $\Delta\theta$, as the mean error in the most-compressive horizontal principal stress orientations given by:

$$\Delta\theta = \frac{1}{N}\sum_{k=1}^{\mathrm{ndat}}[X_{\mathrm{Q}}|\theta_{\mathrm{wsm}}-\theta|]_k$$

where θ_{wsm} is the stress azimuth from the World Stress Map-97 (WSM97 [21], Fig. 3), θ is the calculated stress orientation, and X_{Q} is a weight factor that depends on the data quality. Usually, $\Delta\theta$ shows large values ($>30°$) due to the scarcity of stress determinations and because they are often representative of local structures [22].

(2) $\Delta\omega$, as the mean absolute deviation between the orientation of the slip vectors between the African and the Eurasian plates calculated from a set of 10 earthquakes ([8], Fig. 3) and those obtained from our model. The slip velocities from the numerical model were calculated by considering the average velocity over a 500 km wide strip at each side of the plate boundary.

(3) Normalized strain rate correlation coefficient (SRC) between the logarithm of the seismic strain rate ($\dot{\varepsilon}_{\mathrm{seismic}}$) and the logarithm of the maximum absolute value between the three principal components of the strain rate calculated from the model ($\dot{\varepsilon}$) as:

$$\mathrm{SRC}=\frac{\sum_{i=1}^{N}\left(\log\dot{\varepsilon}_i-\overline{\log(\dot{\varepsilon})}\right)\cdot\left(\log(\dot{\varepsilon}_{\mathrm{seismic}})_i-\log(\dot{\varepsilon}_{\mathrm{seismic}})\right)}{\left[\left(\sum_{i=1}^{N}\left(\log\dot{\varepsilon}_i-\overline{\log(\dot{\varepsilon})}\right)^2\right)\cdot\left(\sum_{i=1}^{N}\left(\log(\dot{\varepsilon}_{\mathrm{seismic}})_i-\overline{\log(\dot{\varepsilon}_{\mathrm{seismic}})}\right)^2\right)\right]^{1/2}}$$

where N is the number of nodes of the grid and the overbar designates the average value of the function over the modelled region. SRC = 1 means a perfect correlation between seismic strain rate and the model results. The seismic strain rate was calculated using the Kostrov method [23] which gives a measure of the brittle deformation according to:

$$\dot{\varepsilon}_{ij} = \frac{1}{2\mu V\Delta t}\sum_{n=1}^{N}(M_0)_{ij}^{(n)}$$

where $\dot{\varepsilon}_{ij}$ is the strain rate, V is the deforming volume, μ is the shear modulus and $(M_0)_{ij}^{n}$ is the seismic moment of the earthquake n-th from the N total earthquakes which occurred during the time interval Δt. The seismic moment is calculated according to Johnston [24]:

$$\log\,[M_0\ (\mathrm{N\ m})] = 11.28 + 1.466\,m_{\mathrm{b}}$$

where m_{b} is the body wave magnitude. To avoid border effects, we enlarged the study area 5° of arc in each direction. Finally, to calculate the seismic strain rate at each node of the grid, we used a Gaussian function such that:

$$\dot{\varepsilon}_{\mathrm{seismic}} = \frac{1}{2\pi\mu L_{\mathrm{s}}b^2\Delta t}\sum_{n=1}^{N}[M_0(N\cdot m)]_n\cdot\exp\left(-\frac{r_n^2}{b^2}\right)$$

where $L_{\mathrm{s}} = 25$ km, r_{n} is the distance to the earthquake n-th, and $\Delta t = 27.08$ yr. Parameter b is the width of the Gaussian function. High values of b would smooth too much the horizontal gradient of the calculated strain rate, whereas small values would restrict the deformation to the vicinity of each epicenter. Several experiments have been

performed in order to choose the most appropiate value which resulted to be $b = 130$ km $\cong$ three times the grid interval.

The best fitting model will be that which shows, simultaneously, the minimum $\Delta\theta$ and $\Delta\omega$, and the maximum SRC.

4. Boundary conditions, plate boundary

The thin-sheet approach requires to define kinematic and/or dynamic boundary conditions and the geometry and properties of the plate boundary. Several authors have constrained the relative velocity between the European and African plates, which can be described as a rotation around an Euler pole, either from global plate motion studies [8,25,26] or from other large-scale investigations [1,2,27,28]. We tested five different rotation poles (Fig. 3) by comparing their model predictions against kinematic data: (1) global model NUVEL-1 [8]; (2) Argus et al. [1]; (3) global model RM2 [26]; (4) global model P071 [25]; (5) McKenzie [27].

We assumed Eurasia as fixed and thereby the boundary conditions are relative to this plate. The generic boundary conditions (Fig. 3) include no motion of the northern boundary and the eastern boundary north of 36°N. The southern boundary and the eastern boundary south of 36°N move according to a particular Africa/Eurasia pole. The ridge-push effect is accounted for by considering the lateral gradient of the potential energy associated with lithospheric thinning inside the modelled region (with 5 km of crustal thickness and −2500 m of elevation). Consequently, we applied as boundary 'force' the potential energy difference between the lithosphere at the western boundary and that corresponding to the oceanic ridge.

In addition to the resulting velocities at the boundaries of the study region, we varied the geometry of the plate boundary and its dynamic properties. For the sake of clarity, in this paper we include only two end-member models among the various tested (Fig. 3). In Model Group A, we considered the geometry of the well known plate boundary from the Azores to the east side of the

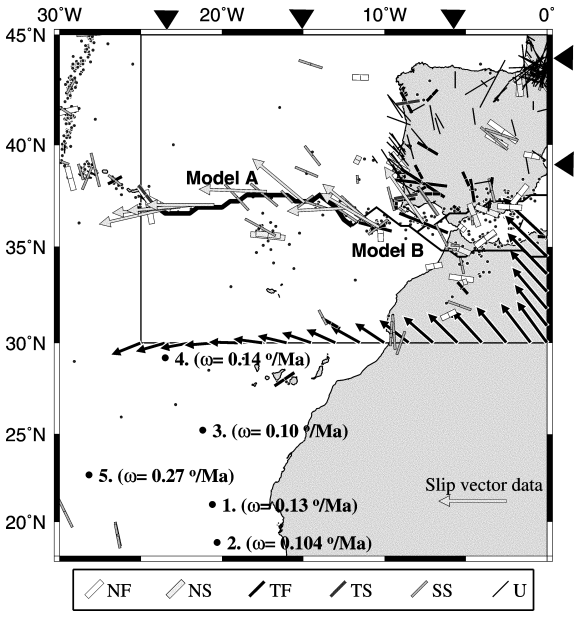

Fig. 3. Most-compressive horizontal principal stress directions from WSM97 [21]. Initials indicate the predominant tectonic regime: NF extension, NS transtension, TF compression, TS transpression, SS strike–slip, and U unknown. Length of symbols is proportional to the quality of data. Arrows correspond to the calculated slip vectors by different authors and compiled on [8]. Circles are earthquake ($m_b \geq 3$) compiled from the ISC Historical Hypocenter Catalog (1964–1991). Geometry of the plate boundary considered in the numerical models: Model A considers a single boundary between Azores and the Gorringe Bank (thick line), Model B considers a single boundary between Azores and the Gorringe Bank (thick line) and a double plate boundary at the Gorringe–Alboran region (thin lines). Generic boundary conditions and location and angular velocities of the considered rotation poles: (1) NUVEL-1 [8]; (2) Argus et al. [1]; (3) RM2 [26]; (4) P071 [25]; (5) McKenzie [27].

Madeira Tore Rise defined from bathymetry and seismicity data [2,3]. This is a continuous plate boundary that only affects the oceanic domain. In Model Group B, we considered that the plate boundary extends further to the east until the eastern boundary of the study region (0°E). This model is supported by several authors who interpreted the Betic–Rif arc in terms of plate tectonics with a third small plate between Africa and Iberia [29,30].

Plate boundaries accommodate most of the plate deformation and, hence, can be regarded

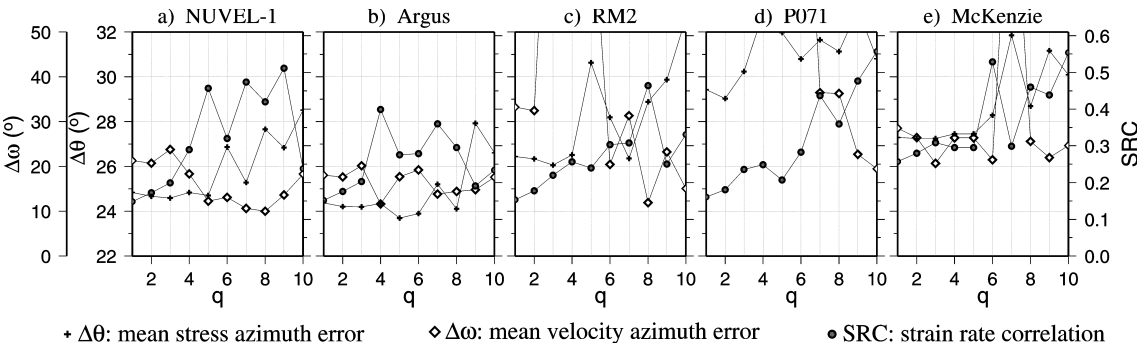

Fig. 4. Scores obtained from Model Group A for different rotation poles and fault coefficients (q). Best models are those with low $\Delta\theta$ and $\Delta\omega$, but high SRC.

as zones of reduced strength. In our numerical approach, plate boundaries are simulated by reducing the lithospheric strength in those nodes that coincide with the pre-defined boundary. We defined a fault coefficient (q) as the ratio of the strength of the lithosphere (calculated from its structure and thermal regime) to the reduced strength assigned to the plate boundary. Thus, high values of q are associated with very weak plate boundaries, whereas $q=1$ would correspond to a continuum lithosphere although the relationship between q and strain rate is highly non-linear. Since the UHURU code is based on finite differences, the width of the modelled plate boundary coincides roughly with the mesh interval (about 0.3°).

5. Results

5.1. Model Group A

Different models were calculated by using five alternative rotation poles proposed for the area and by varying the fault coefficient (q) from 1 to 10. The resulting maximum compressive stress orientations, seismic strain rates, and slip vectors are compared with those values deduced from experimental data (Fig. 4).

From Fig. 4, we can infer that despite the oscillations observed in the scores which are related to the scarcity of data, both NUVEL-1 and Argus' poles show similar results with a plausible range of fault coefficient between $q=4$ and $q=7$. In contrast, the Euler poles given by models P071 [25] and RM2 [26] are located closer to the plate boundary and hence, the transition from a convergent to a divergent plate boundary is produced in a narrower region resulting in a higher misfit of $\Delta\theta$ and $\Delta\omega$. The Euler pole proposed by McKenzie [27] is located to the west of the study region and therefore cannot reproduce divergence along the studied segment of the plate boundary.

Fig. 5 shows the maximum strain rates and the orientation of the principal stresses obtained from the numerical model, for the Argus' pole and $q=4$. Maximum deformation is concentrated along the plate boundary. East of the Madeira Tore Rise, the resulting strain rate is slightly lower and deformation spreads over a wide region affecting the SW margin of Iberia and the northwestern margin of Morocco. On land, numerical results show that deformation concentrates mainly in North Africa, along the Atlas chain and, partly, in the southern margin of the Alboran basin. This contrasts with the low strain rates obtained in the Iberian Peninsula, where deformation is restricted to its southwestern domain. Near the Azores, the major horizontal principal stress is tensional with a NNE–SSW direction, resulting in a transtensional tectonic regime. Along the Gloria fault, the dominant tectonic regime is strike–slip with a small component of compression oriented NW–SE. To the east, the compression direction becomes NNW–SSE and the strain rate includes a larger component of reverse faulting. These results are in good agreement with those obtained from focal mechanisms analyses [2,3].

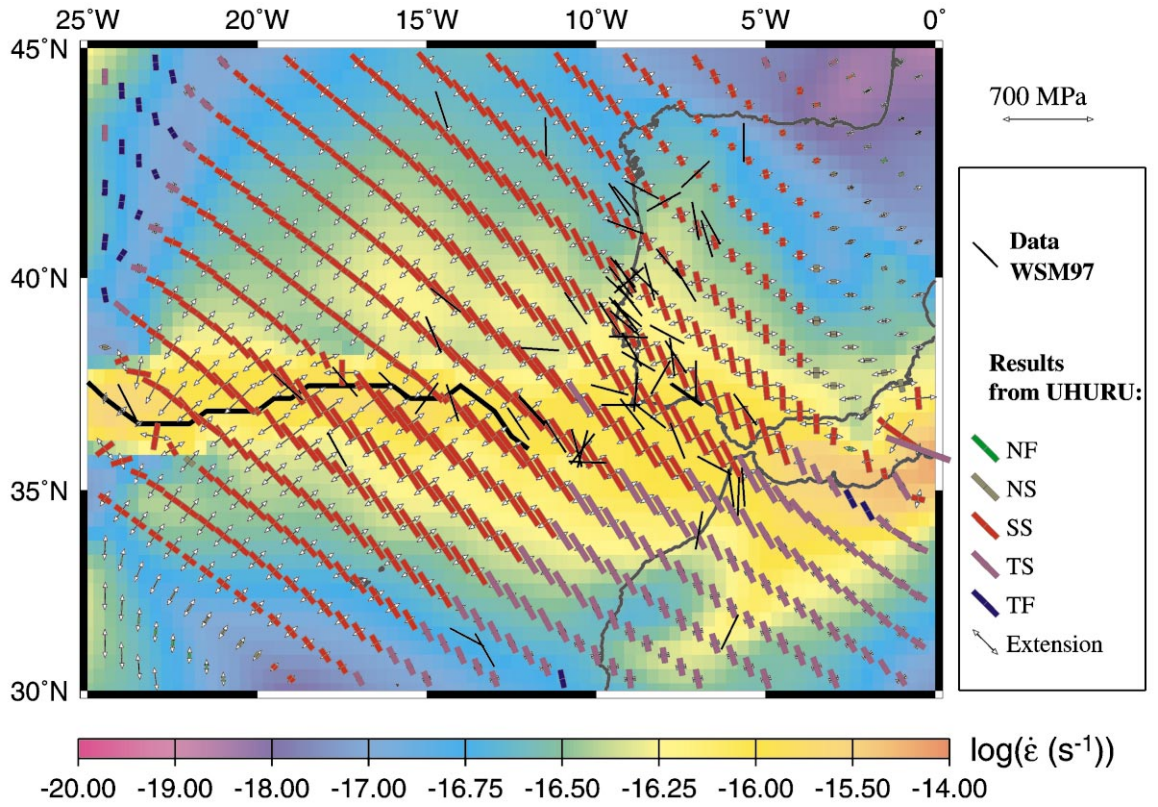

Fig. 5. Maximum absolute strain rate (log($\dot{\varepsilon}(s^{-1})$) and horizontal principal stress directions from Model Group A considering the Argus et al. rotation pole [1] and a fault coefficient of $q=4$. Initials as in Fig. 3.

5.2. Model Group B

A variety of geodynamic models have been proposed to explain the origin and evolution of the Alboran basin and the Betics and Rif chains [29,31–33]. The lack of consensus on the kinematic evolution of the Alboran domain makes us to consider three different boundary conditions at the easternmost border of this region (between 34.5°N and 37.5°N): (a) a 'free' boundary (subject only to normal lithostatic tractions); (b) an imposed westward velocity (2.6 mm yr^{-1}); and (c) an imposed velocity resulting from the rotation pole. The first boundary condition (Model B1) makes the displacement of the Alboran domain to result from the viscous drag of the African plate, and the plate boundary is located predominantly in North Africa. The second boundary condition (Model B2) tends to force both the south Iberian and the North African margins to act as plate boundaries, so that the Alboran domain behaves as an independent microplate [29,30]. Finally, the third boundary condition (Model B3) tends to force the Alboran domain

→

Fig. 6. (a–c) Scores obtained from Model Group B using the rotation pole of Argus [1]. The fault strength coefficient is set to $q=7$ to the western segment of the plate boundary and varies from $q_E=1$ to 3 in the easternmost segment. See text for differences between Model Groups B1, B2 and B3. (d–f) Strain rate and velocity fields obtained from the best models in Groups B1 ($q_E=2.0$), B2 ($q_E=1.2$), and B3 ($q_E=1.4$). White thick arrows indicate the velocity boundary conditions imposed to each model. Velocities (black thin arrows) less than 0.5 mm yr^{-1} are not plotted.

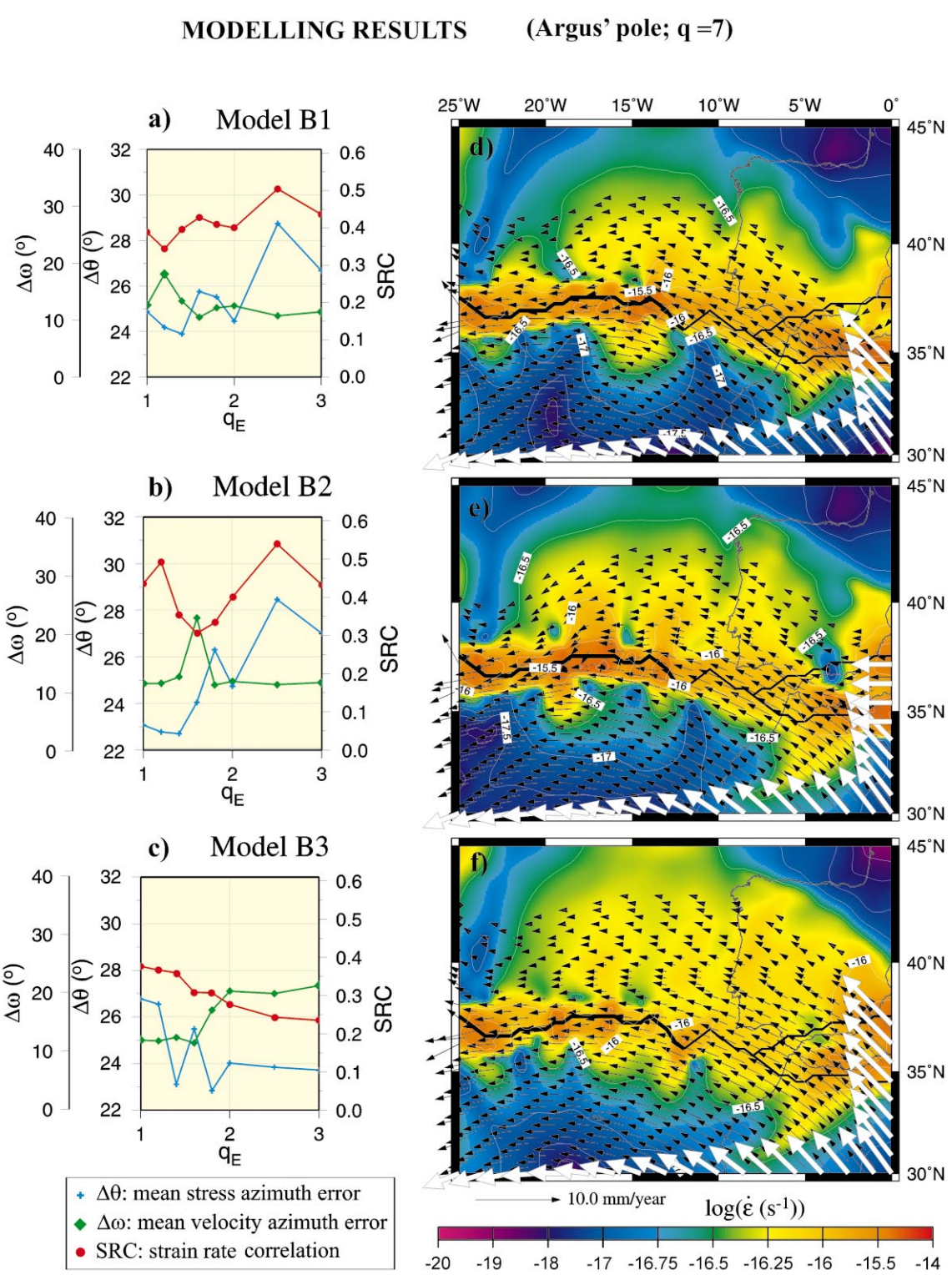
MODELLING RESULTS (Argus' pole; q =7)
a) Model B1
b) Model B2
c) Model B3
Δω (°)
Δθ (°)
SRC
q_E
Δθ: mean stress azimuth error
Δω: mean velocity azimuth error
SRC: strain rate correlation
25°W
20°W
15°W
10°W
5°W
0°
45°N
40°N
35°N
30°N
d)
e)
f)
10.0 mm/year
log(ε̇ (s⁻¹))
-20 -19 -18 -17 -16.75 -16.5 -16.25 -16 -15.5 -14

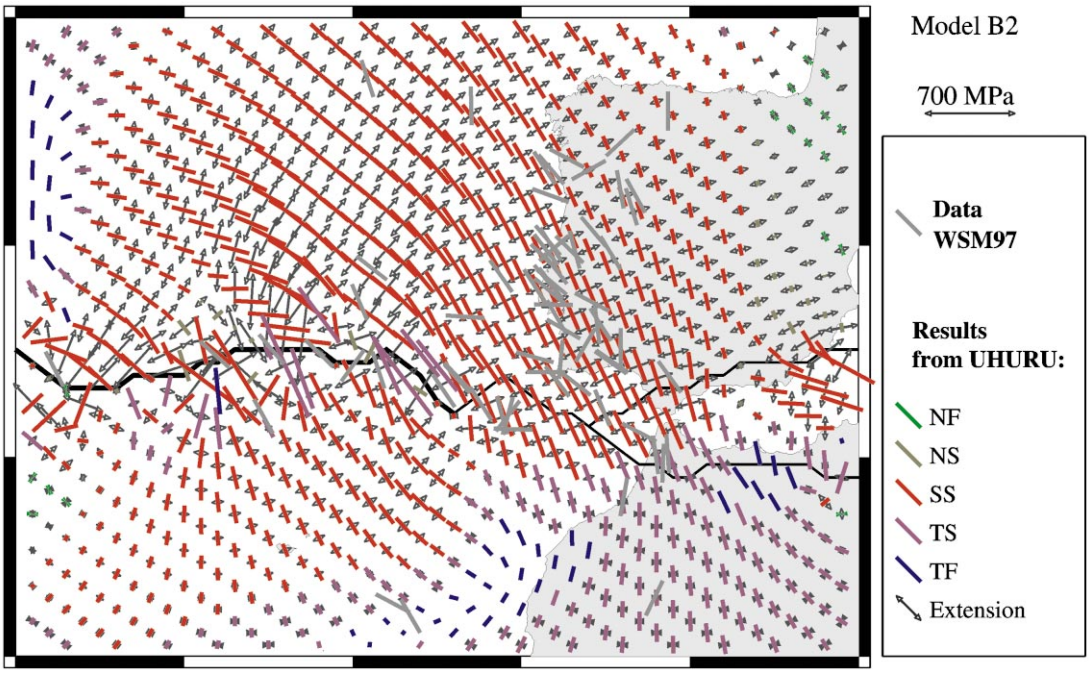

Fig. 7. Principal stress directions obtained from Model B2 with $q = 7$ and $q_E = 1.2$. Initials as in Fig. 3.

to move jointly with the African plate and favors the Iberian margin as the predominant plate boundary.

For simplicity, we show only the effects of different fault coefficients (q_E) to the eastern segment of the plate boundary (east of the Gorringe Bank) with Argus' rotation pole provided that no significant differences are found with respect to the NUVEL-1 pole. Furthermore, in contrast to the best models of Group A, the fault coefficient along the western and central segments of the plate boundary must be set to $q = 7$. Fig. 6a–c shows that the best fitting models require a fault coefficient applied to the eastern segment restricted to values between 1.2 and 2, depending on the boundary condition.

The strain rate distributions obtained in Model B1 and Model B2 (Fig. 6d,e) show deformation concentrating mainly in the African plate whereas Iberia remains almost undeformed. The deformation produced by the convergence of Africa against Iberia is mainly accommodated by the Alboran domain, and its weakness prevents a lot of stress propagation across Iberia and its western margin. Model B2 (Fig. 6e), with SRC = 0.5 and $\Delta\theta < 23°$ for $q = 1.2$, best reproduces the transition from a linear and narrow plate boundary to a diffuse plate boundary. The resulting maximum strain rate is concentrated along the Gloria fault, and strain becomes more diffuse to the east, from the Madeira Tore Rise to the Gulf of Cadiz region. Actually, deformation should affect the Tagus Abyssal Plain and the southwestern part of the Iberian Peninsula, in good agreement with recent neotectonic analyses [6,34]. In contrast, Model B3 (Fig. 6f) creates more strain propagation through the Eurasian plate, which results in more deformation in the Iberian Peninsula and also in its western margin and the oceanic domain. This propagation of deformation through the Eurasian plate produces a lower strain rate near the plate boundary, which results in a poor correlation with the seismic strain rate.

The regional stress regime resulting from Model B2 is shown in Fig. 7. In the eastern segment of the plate boundary the tectonic regime is mainly transpressive, in agreement with seismicity [2,3,35] and seismic reflection data [34,36]. In the vicinity

of the Gorringe Bank, the modelled stress distribution shows a larger compression with thrust tectonics. The area is a highly fractured zone [12] which has been interpreted either as an uplifted lithospheric block [37] or the initiation of subduction zone [6]. Further to the west, along the Gloria fault, the calculated stress regime is predominantly strike–slip with a NW orientation, whereas NNE tension dominates in the Terceira ridge. This regional tectonic stress field along the Azores–Gibraltar plate boundary agrees with the results obtained from focal mechanisms [2,3,38].

6. Discussion

The major goals of our study were to reproduce the stress regime of the Azores–Gibraltar plate boundary, and to analyze the transition from a linear to a diffuse plate boundary. To this end, we used a thin-sheet numerical approach under the approximation that the lithosphere behaves as a viscous fluid. The study region contains oceanic lithosphere with ages from a few Myr to about 120–140 Myr, and also includes transitions to cratonic and Hercynian continental lithospheres in Africa and Iberia, respectively. This heterogeneity may imply large lateral variations of the total lithospheric strength. We made a rough estimate of the crustal and lithospheric structure, using global elevation data and available surface heat flow and seismic data, under the assumptions of local isostasy and thermal equilibrium. These conditions are not strictly fulfilled over the whole region and could cause local departures from the proposed lithospheric structure. Likewise, rock deformation experiments give a wide range of rheological parameters depending on the rock deformed. However, to the extent that plate tectonics are controlled by regional variations of the total lithospheric strength and gravitational potential energy, these models may succeed despite possible systematic errors in the rock type and geotherms assumed. According to the chosen rheological parameters, the total lithospheric strength in the region is about $30 \pm 10 \times 10^{12}$ N m, which is much higher than the forces associated with variations of the gravitational potential energy ($\sim 2 \pm 1 \times 10^{12}$ N m). Thereby, only in the case of choosing a very soft rheology lateral variations in crustal and lithospheric mantle thickness can play a predominant role in lithospheric deformation in this region.

Our numerical results were compared with the seismic strain rate, the maximum compressive stress directions, and the orientation of slip vectors. Unfortunately, the available data are scarce and observations are mainly restricted to areas with recent seismicity, which makes it difficult to have full confidence in the relative scoring of the models. Actually, the abrupt changes in SRC, $\Delta\theta$ and $\Delta\omega$ related to plate velocity and/or fault coefficient variations are due to the lack of more widespread data rather than to numerical instabilities, which have been properly checked. Bearing in mind these limitations, the best fitting models, regardless of the geometry of the plate boundary east of the Gorringe Bank, are those using the rotation pole of Argus et al. [1] and the global NUVEL-1 model [8]. Rotation poles deduced from the global models, RM2 [26] and P071 [25], result in worse SRC and also in larger $\Delta\theta$, and must be discarded.

In all the models, the linear segment of the plate boundary from the Azores to the Gorringe Bank is characterized by an average lithospheric strength between four and seven times lower than that inferred from its lithospheric structure ($q = 4$–7). This fault coefficient corresponds to reduce the frictional sliding coefficient from 0.85 to 0.13–0.06, assuming the same ductile parameters. These values of frictional sliding are close to the average values of 0.03–0.05 proposed by Bird [22] for plate boundaries in a global tectonic model. The fact that the Azores–Gorringe boundary developed along an ancient major transcurrent fault inherited from the Hercynian orogeny could result in an anisotropic mantle viscosity leading to a directional strain softening [39]. The observed aseismicity of the Gloria fault is not reproduced by our models, which can be attributed to either a viscous behavior of this segment or to the short (in geological time) seismic catalog.

Model Group B considers that the prolongation of the plate boundary towards the Gibral-

tar–Alboran region results in a double boundary lying along the Betic and Rif chains. In this region, the optimal fault coefficient is $q = 1.2–1.6$, corresponding to a frictional sliding coefficient of about 0.6–0.3. These values are considerably higher than that obtained for the Azores–Gorringe segment, which implies that the eastern part of the plate boundary is not as much weakened. Seismic data recorded at the Gorringe–Gibraltar segment [34] show that the area from the southern Tagus Plain to the northern Seine Plain is affected by low angle thrust faults and folding. These authors show that the distribution of active vs. inactive elements does not show a clear space–time correlation and conclude that shortening is accommodated over an area wider than 200 km. The evidence that most of the transpressive deformation is accommodated by a widespread fault system, rather than by a single fault structure, as proposed also by Morel and Meghraoui [7] from seismicity data, favors a higher frictional sliding coefficient (lower fault coefficient). Neotectonic studies carried out in complex fault systems associated with plate boundaries in California and Alaska yield frictional coefficient values of about 0.17 [40,41]. These values are close to those obtained in our study and are noticeably higher than the values of 0.03–0.05 obtained for global plate boundaries [22].

We applied different boundary conditions on the eastern boundary of the Alboran domain to analyze how the stress propagation between the African and the Eurasian plates operates, and its influence on the Azores–Gibraltar plate boundary. However, the results concerning the tectonics of the Alboran domain are very qualitative because this region is close to the limit of the study area. In addition, we have considered neither local structural features nor stresses produced by sublithospheric processes such as sinking of a broken-off slab or mantle delamination. Despite that, some conclusions can be drawn. Model Groups B1 and B2 show similar scores although the best fits are obtained in Group B2, which enforces an independent westward velocity of the Alboran domain, as proposed by several authors [29,30]. This imposed velocity causes compression to propagate towards the Gorringe–Gibraltar region and the southwestern Iberian Peninsula, in good agreement with observations. In Model B1, the Alboran domain is dragged by the African plate. The brittle expression of this dragging would support the idea of a half-pinned model [7], in which the African plate and the blocks of the Gorringe–Alboran–Tell region are fixed resulting in a right lateral transpression system. In contrast, Model B3 yields unacceptable results since stresses are propagated too far towards the interior of the Eurasian plate.

The change from a linear to a diffuse plate boundary is probably due to the following factors: (a) the transition from oceanic to continental lithosphere, (b) the weakness of the hot and thin lithosphere of the Alboran domain, (c) the predominant compressive–transpressive tectonic regime in this region, and/or (d) a more complex geologic history in the Alboran region, with multiple inherited planes of weakness. However, the similarity of the scores obtained from Model Groups A, B1 and B2 suggests that, although the geometry of the plate boundary in the Gorringe–Alboran area may play a major role in local neotectonic studies, it has a second order effect on the regional mode of deformation.

Acknowledgements

The authors thank the valuable comments by Scott King, G. Houseman and an anonymous reviewer which helped us to improve the manuscript version. Financial support has been obtained from the Spanish agencies DGICYT (PB94-0013), CICYT (MAR98-0962) and CIRIT (1999 SGR00208).*[SK]*

Appendix

A.1. Mechanical model

The equilibrium equation for a viscous lithosphere is given by:

$$\frac{\partial \sigma_{ij}}{\partial x_j} = \rho g_i,\ i, j = 1, 2, 3 \qquad \text{(A1.1)}$$

where g is the acceleration due to gravity and $\sigma_{ij}=\tau_{ij}+1/3\delta_{ij}\sigma_{kk}$ is the total stress; σ_{kk} is the sum of the terms of the diagonal from the stress tensor, $\sigma_{kk}=\sigma_{11}+\sigma_{22}+\sigma_{33}$, and $\delta_{ij}=1$ if $i=j$ and $\delta_{ij}=0$ if $i\neq j$. The deviatoric stress, τ_{ij}, is related to the strain rate through the constitutive equation:

$$\overline{\tau}_{ij}=2\eta\dot{\varepsilon}_{ij},\ i,\ j=1,\ 2,\ 3 \tag{A1.2}$$

where η is the effective viscosity and $\dot{\varepsilon}_{ij}$ is the strain rate tensor. Assuming that the vertical variations of the horizontal velocity components are negligible [42] the vertically averaged deviatoric stress is:

$$\overline{\tau}=\frac{1}{L}\int_0^L \mathrm{d}z=\frac{1}{L}F_{\mathrm{lit}} \tag{A1.3}$$

where L is the lithospheric thickness and F_{lit} is the total lithospheric strength that results from the depth integral of the stress envelope for a given strain rate. The stress envelope is given by the lesser of the brittle and ductile stresses. The frictional sliding is a function of the depth (z), according to $\tau_{\mathrm{brittle}}=\beta z$, and for ductile deformation:

$$\tau_{\mathrm{ductile}}=\left(\frac{\dot{\varepsilon}}{A}\right)^{1/n}\exp\left(\frac{Q}{nRT}\right),\ \tau\leq 200\ \mathrm{MPa}$$

$$\tau_{\mathrm{ductile}}=\sigma_{\mathrm{D}}\left[1-\left(\frac{RT}{Q_{\mathrm{D}}}\ln\left(\frac{\dot{\varepsilon}_{\mathrm{D}}}{\dot{\varepsilon}}\right)\right)^{1/2}\right],\ \tau>200\ \mathrm{MPa}$$

where A, Q, n, σ_{D}, Q_{D} and $\dot{\varepsilon}_{\mathrm{D}}$ are material constants and they depend of the type of the rock, R is the gas constant, and T is absolute temperature. When stresses are higher then 200 MPa according to [43] we use the Dorn law. The effective viscosity depends on the temperature and velocity and is calculated from the depth integral of the stress envelope.

As a result of the thin-sheet approach and considering that the fluid is incompressible, Eq. A1.1 yields:

$$\frac{\partial}{\partial x_j}\left[\eta\left(\frac{\partial u_i}{\partial x_j}+\frac{\partial u_j}{\partial x_i}\right)\right]+\frac{\partial}{\partial x_i}\left[2\eta\left(\frac{\partial u_1}{\partial x_1}+\frac{\partial u_2}{\partial x_2}\right)\right]=\frac{\partial\overline{p}}{\partial x_i}$$

where i, j = 1, 2 are the horizontal components; u_1 and u_2 are horizontal components of the velocity vector; and $\overline{p}$ is vertically averaged until the maximum depth reached by the lithosphere over the study region to include the gravitational potential energy variations induced by lateral variations in crustal and lithospheric mantle thicknesses.

A.2. Elevation, surface heat flow and crustal and lithospheric thicknesses

Under the assumption of local isostasy and steady-state thermal regime, the elevation of a given lithospheric column can be expressed as [44]:

$$e=\frac{\rho_{\mathrm{a}}-\rho_{\mathrm{l}}}{\rho_{\mathrm{a}}}L-H_0,\ \mathrm{e}\geq 0 \tag{A2.1}$$

$$e=\frac{\rho_{\mathrm{a}}}{\rho_{\mathrm{a}}-\rho_{\mathrm{w}}}\left(\frac{\rho_{\mathrm{a}}-\rho_{\mathrm{l}}}{\rho_{\mathrm{a}}}L-H_0\right),\ \mathrm{e}<0$$

where L is the lithospheric thickness, ρ_{w}, ρ_{l}, and ρ_{a} are, respectively, the densities of water, lithosphere and asthenosphere, and $H_0=2400$ m. However:

$$\rho_{\mathrm{l}}=\frac{\rho_{\mathrm{c}}s+\rho_m h_{\mathrm{m}}}{L} \tag{A2.2}$$

where ρ_{c} and s, and ρ_{m} and h_{m} are, respectively, the densities and thicknesses of the crust and the lithospheric mantle, and therefore:

$$s=\frac{\rho_{\mathrm{a}}}{\rho_{\mathrm{a}}-\rho_{\mathrm{c}}}\left(e-\frac{\rho_{\mathrm{a}}-\rho_{\mathrm{m}}}{\rho_{\mathrm{a}}}h_{\mathrm{m}}+H_0\right),\ e\geq 0 \tag{A2.3}$$

$$s=\frac{\rho_{\mathrm{a}}}{\rho_{\mathrm{a}}-\rho_{\mathrm{c}}}\left(\frac{\rho_{\mathrm{a}}-\rho_{\mathrm{w}}}{\rho_{\mathrm{a}}}e-\frac{\rho_{\mathrm{a}}-\rho_{\mathrm{m}}}{\rho_{\mathrm{a}}}h_{\mathrm{m}}+H_0\right),\ e<0$$

which relates the crustal thickness (s) with elevation and the lithospheric mantle thickness (h_{m}). We considered that the density of the mantle is temperature dependent:

$$\rho_{\mathrm{m}}=\rho_{\mathrm{a}}\left(1+\frac{\alpha}{2}(T_{\mathrm{a}}-T_{\mathrm{moho}})\right) \tag{A2.4}$$

where α is the thermal expansion coefficient of the lithospheric mantle.

Since the base of the lithosphere is assumed to coincide with the 1300°C isotherm, L and h_m can be calculated from:

$$-K\frac{d^2T}{dz^2}=H \tag{A2.5}$$

where K is the thermal conductivity and H is the radiogenic heat production. Considering that in the crust $H=H_{sup}\exp(-z/b)$ and in the lithospheric mantle $H=H_m$, Eq. A2.6 yields:

$$T_c(z)=$$

$$T_{sup}+\frac{1}{K_c}\left[(Q_{sup}-H_{sup}b)z+H_{sup}b^2\left(1-\exp\left(-\frac{z}{b}\right)\right)\right],$$

$$z\leq s \tag{A2.6}$$

$$T_m(z)=T_{moho}+\frac{Q_{moho}}{K_m}(z-s)-\frac{H_m}{2K_m}(z-s)^2,\quad z>s$$

where c and m are referred to crust and mantle, respectively, Q_{sup} and Q_{moho} and T_{sup} and T_{moho} are the heat flow and temperatures at the surface and the base of the crust. Therefore, combining Eqs. A2.3 and A2.6 we can calculate s and h_m knowing e and Q_{sup} or, alternatively, knowing e and s we can calculate Q_{sup} and h_m.

References

[1] D.F. Argus, R.G. Gordon, C. DeMets, S. Stein, Closure of the Africa–Eurasia–North America plate motion circuit and tectonics of the Gloria fault, J. Geophys. Res. 94 (1989) 5585–5602.

[2] E. Buforn, A. Udías, M.A. Colombás, Seismicity, source mechanisms and tectonics of the Azores–Gibraltar plate boundary, Tectonophysics 152 (1988) 89–118.

[3] N. Grimison, W. Chen, The Azores–Gibraltar plate boundary: focal mechanisms, depths of earthquakes, and their tectonic implications, J. Geophys. Res. 91 (1986) 2029–2047.

[4] M. Torne, M. Fernàndez, M.C. Comas, J.I. Soto, Lithospheric structure beneath the Alboran basin: Results from 3D gravity modeling and tectonic relevance, J. Geophys. Res. 105 (2000) 3209–3228.

[5] C. Pierce, P. Barton, Crustal structure of the Madeira-Tore Rise, eastern North Atlantic – results of a DOBS wide-angle and normal incidence seismic experiment in the Josephine Seamount region, Geophys. J. Int. 106 (1991) 357–378.

[6] A. Ribeiro, J. Cabral, R. Baptista, L. Matias, Stress pattern in Portugal mainland and the adjacent Atlantic region, West Iberia, Tectonics 15 (1996) 641–659.

[7] J.L. Morel, M. Meghraoui, Gorringe–Alboran–Tell tectonic zone: A transpression system along the Africa–Eurasia plate boundary, Geology 24 (1996) 755–758.

[8] C. DeMets, R.G. Gordon, D.F. Argus, S. Stein, Current plate motions, Geophys. J. Int. 101 (1990) 425–478.

[9] H.N. Pollack, S.J. Hurter, J.R. Johnson, Heat loss from the Earth's interior: analysis of the global data set, Rev. Geophys. 31 (1993) 267–280.

[10] M. Fernàndez, I. Marzán, A. Correia, E. Ramalho, Heat flow, heat production, and lithospheric thermal regime in the Iberian Peninsula, Tectonophysics 291 (1998) 29–53.

[11] B. Parsons, J.G. Sclater, An analysis of the variation of ocean floor bathymetry and heat flow with age, J. Geophys. Res. 82 (1977) 803–827.

[12] A. Bergeron, J. Bonnin, The deep structure of Gorringe Bank (EN Atlantic) and its surrounding area, Geophys. J. Int. 105 (1991) 491–502.

[13] M. Torné, M. Fernàndez, J. Carbonell, E. Banda, Lithospheric transition from continental to oceanic in the west Iberia Atlantic margin, in: E. Banda, M. Torné, M. Talwani (Eds.), Rifted Ocean–Continent Boundaries, NATO ASI series, Kluwer Academic Publishers, 1995, pp. 247–263.

[14] V. García-Dueñas, E. Banda, M. Torné, D. Córdoba, the ESCI-Béticas Working Group, A deep seismic reflection survey across the Betic Chain (southern Spain): first results, Tectonophysics 232 (1994) 77–89.

[15] E. Sandvol, D. Seber, M. Barazangi, Single-station receiver function inversions in the Middle East and North Africa: A grid search approach, EOS Trans. AGU 77 (1996) 46477.

[16] G. Shelton, J. Tullis, Experimental flow law for crustal rocks, EOS Trans. AGU 62 (1981) 396.

[17] D.L. Kohlstedt, C. Goetz, Low-stress high-temperature creep in single olivine crystals, J. Geophys. Res. 79 (1974) 2045–2051.

[18] H.D. Lynch, P. Morgan, The tensile strength of the lithosphere and the localization of extension, in: M.P. Coward, J.F. Dewey and P.L. Hancock (Eds.), Continental Extension Tectonics, Geol. Soc. London Spec. Publ. 28, 1987, pp. 53–65.

[19] A. Tommasi, A. Vauchez, B. Daudré, Initiation and propagation of shear zones in a heterogeneous continental lithosphere, J. Geophys. Res. 100 (1995) 22083–22101.

[20] E. Neil, G. Houseman, Geodynamics of the Tarim Basin and the Tian Shan in central Asia, Tectonics 16 (1997) 571–584.

[21] B. Mueller, V. Wehrle, K. Fuchs, The 1997 release of the

World Stress Map, 1997 (available on-line at http://www-wsm.physik.uni-karlsruhe.de/pub/Rel97/wsm97.html).
[22] P. Bird, Testing hypotheses on plate-driving-mechanism with global lithosphere models including topography, thermal structure, and faults, J. Geophys. Res. 103 (1998) 10115–10129.
[23] V. Kostrov, Seismic moment and energy of earthquakes, and seismic flow of rock, Izv. Acad. Sci. USSR Phys. Solid Earth 1 (1974) 23–44.
[24] A.C. Johnston, Seismic moment assessment of earthquakes in stable continental regions – I. Instrumental seismicity, Geophys. J. Int. 124 (1996) 381–414.
[25] C.G. Chase, Plate kinematics: the Americas, east Africa, and the rest of the world, Earth Planet. Sci. Lett. 37 (1978) 355–368.
[26] J.B. Minster, T.H. Jordan, Present-day plate tectonics, J. Geophys. Res. 83 (1978) 5331–5354.
[27] D.P. McKenzie, Active tectonics of the Mediterranean region, Geophys. J. R. Astron. Soc. 30 (1972) 109–185.
[28] D. Albarello, E. Mantovani, D. Babbucci, C. Tamburelli, Africa–Eurasia kinematics: main constraints and uncertainties, Tectonophysics 243 (1995) 25–36.
[29] J. Andrieux, J.M. Fontobé, M. Durand-Delga, Sur un modèle explicatif de l'Arc de Gibraltar, Earth Planet. Sci. Lett. 12 (1971) 191–198.
[30] J.C. Balanya, V. Garcia-Dueñas, Les directions structurales dans le Domaine d'Alboran de part et d'autre du Detroit de Gibraltar, C.R. Acad. Sci. Ser. 2 304 (1987) 929–933.
[31] V. García-Dueñas, J.C. Balanya, J.M. Martinez-Martinez, Miocene extensional detachments in the outcropping basement of the northern Alboran basin (Betics) and their tectonic implications, Geomar. Lett. 12 (1992) 88–95.
[32] C. Docherty, E. Banda, Evidence for the eastward migration of the Alboran Sea based on regional subsidence analysis: A case for basin formation by delamination of the subcrustal lithosphere?, Tectonics 14 (1995) 804–818.
[33] R.L. Vissers, J.P. Platt, D. VanderWal, Late orogenic extension of the Betic Cordillera and the Alboran Domain: A lithospheric view, Tectonics 14 (1995) 786–803.
[34] R. Sartori, L. Torelli, N. Zitellini, D. Peis, E. Lodolo, Eastern segment of the Azores–Gibraltar line (central–eastern Atlantic): An oceanic plate boundary with diffuse compressional deformation, Geology 22 (1994) 555–558.
[35] F. Medina, Present-day state of stress in northern Morocco from focal mechanism analysis, J. Struct. Geol. 17 (1995) 1035–1046.
[36] D. Tortella, M. Torné, A. Pérez-Estaún, Geodynamic evolution of the eastern segment of the Azores–Gibraltar zone: The Gorringe Bank and the Gulf of Cadiz region, Mar. Geophys. Res. 19 (1997) 211–230.
[37] J.M. Auzende, J. Charvet, A. LeLann, X. LePichon, J.H. Monteiro, A. Nicolas, J.L. Olivet, A. Ribeiro, Sampling and observation of oceanic mantle and crust on Gorringe Bank, Nature 273 (1978) 45–49.
[38] A. Kiratzi, C.B. Papazachos, Active crustal deformation from the Azores triple junction to the Middle East, Tectonophysics 243 (1995) 1–24.
[39] A. Tommasi, A. Vauchez, Continental rifting parallel to ancient collisional belts: an effect of the mechanical anisotropy of the lithospheric mantle, Earth Planet. Sci. Lett. 185 (2001) 199–210.
[40] P. Bird, X. Kong, Computer simulations of California tectonics confirm very low strength of major faults, Geol. Soc. Am. Bull. 106 (1994) 159–174.
[41] P. Bird, Computer simulations of Alaskan neotectonics, Tectonics 15 (1996) 225–236.
[42] P.C. England, D.P. McKenzie, Correction to: A thin viscous sheet model for continental deformation, Geophys. J. R. Astron. Soc. 73 (1983) 523–532.
[43] C. Goetze, B. Evans, Stress and temperature in the bending lithosphere as constrained by experimental rock mechanics, Geophys. J. R. Astron. Soc. 59 (1979) 463–478.
[44] A. Lachenbruch, P. Morgan, Continental extension, magmatism and elevation; formal relations and rules of thumb, Tectonophysics 174 (1990) 39–62.